Gravity segregation with CO2 foam in heterogeneous reservoirs

Lyu, X.; Voskov, D.; Rossen, W.

DOI
10.3997/2214-4609.202133029

Publication date
2021

Document Version
Final published version

Published in
IOR 2021 - 21st European Symposium on Improved Oil Recovery

29

Gravity Segregation with CO2 Foam in Heterogeneous Reservoirs

X. Lyu[1], D. Voskov[1,2], W. Rossen[1]

[1] Delft University of Technology; [2] Stanford University

Summary

Foam injection is one efficient way to mitigate gravity segregation during CO2 injection into porous media. The effect of gravity segregation on foam propagation in heterogeneous porous media is not yet fully resolved. To assess CO2 foam transport for enhanced oil recovery (EOR) and for CO2 storage processes in heterogeneous reservoirs, an accurate prediction of foam behavior is essential. In this study, we investigate the effect of heterogeneity on gravity segregation in the presence of foam. For nonlinear analysis, we use an extension of an Operator-Based Linearization (OBL) approach proposed recently. The OBL approach helps to reduce the nonlinearity of complex physical problems by transforming the discretized nonlinear conservation equations into a quasi-linear form based on state-dependent physical operators. The state-dependent operators are approximated by discrete representation on a uniform mesh in parameter space. In our study, foam in porous media is described using an implicit-texture (IT) foam model with two flow regimes.

We first validate the numerical accuracy of the foam simulation with OBL by comparing segregation length using the IT foam model with Newtonian rheology to analytical solutions. Next, the foam-model parameters are fit to foam-quality scan data for four sandstone formations ranging in permeability by an order of magnitude using a least-squares optimization approach. We then construct several hypothetical models containing two communicating layers with different permeability and thickness ratios to examine foam's effect on gravity segregation.

The numerical results of the segregation length in homogeneous domains show good agreement with analytical solutions, except in a transition zone beneath the override zone which is not included in the analytical model. Through fractional-flow theory, we find that the transition zone is not a numerical artefact, but caused by low gas relative-mobility during the transient displacement process. Permeability affects both the mobility reduction of wet foam in the low-quality regime and the limiting capillary pressure at which foam collapses. Thus the segregation length varies with permeability and foam strength. In two-layer models, the thickness of the top layer plays an important role in the ultimate segregation length. A thin top layer does not affect segregation in the bottom layer, while a thicker top layer dominates the segregation length, with less influence of the bottom layer.

Introduction

Gas injection can displace oil where gas sweeps (Lake et al., 2014). The gas phase (commonly N_2, CO_2, produced hydrocarbon gas, or a combination of these) is injected into reservoirs either as a miscible or immiscible displacement process. However, due to reservoir heterogeneity, gravity override, and viscous instability, gas injection typically suffers from poor sweep efficiency. Foam, an agglomeration of gas bubbles separated from each other by thin liquid films, can overcome these problems and thereby improve the sweep efficiency in gas-injection EOR processes (Schramm, 1994; Rossen, 1996; Dholkawala et al., 2007) or enlarge the storage space for trapping of CO_2 (Talebian et al., 2013; Vitoonkijvanich et al., 2015; Lyu et al., 2020).

Stone (1982) presented a steady-state analytical model for gas sweep in uniform co-injection of water and gas into homogeneous, horizontal reservoirs. This model can also be applied to water-alternating-gas (WAG) injection as long as injection cycles are short enough to guarantee that all slugs can mix thoroughly near the well. Besides, Stone (1982) assumed that at steady state three regions of uniform saturation can be distinguished in a reservoir, with sharp boundaries between them: an override zone with only gas flowing, an underride zone with only water flowing, and a mixed zone adjacent to the wellbore with both gas and water flowing (Fig. 1).

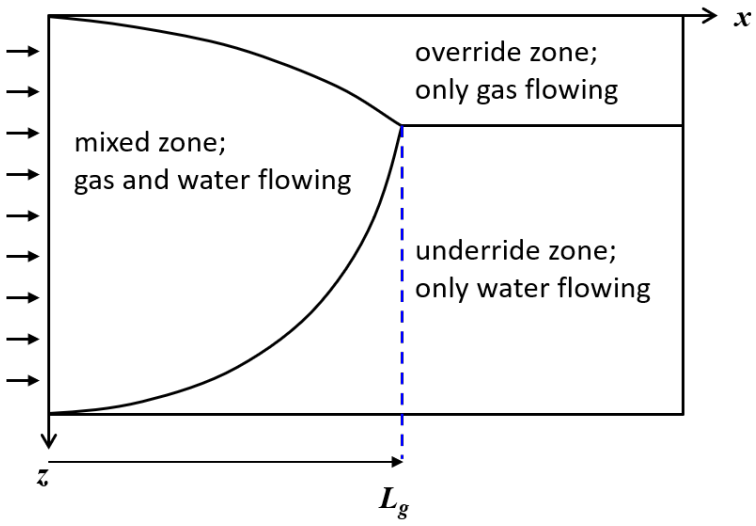

Figure 1 *Schematic of three uniform zones at steady state in the gravity-segregation model of Stone (1982) and Jenkins (1984) for continuous co-injection of water and gas. L_g is the ultimate distance where gas and water completely segregate.*

The distance between the injection well and the point where the mixed zone disappears is called the segregation length (L_g). Stone (1982) and Jenkins (1984) derived equations for L_g (in a rectangular reservoir) or R_g (in a cylindrical reservoir):

$$L_g = \frac{Q_t}{k_z(\rho_w - \rho_g)gW\lambda_{rt}^m} \tag{1}$$

$$R_g = \sqrt{\frac{Q_t}{\pi k_z(\rho_w - \rho_g)g\lambda_{rt}^m}} \tag{2}$$

where Q_t is the total volumetric injection rate of gas and water, k_z vertical permeability, ρ_w and ρ_g densities of water and gas respectively, g the gravitational acceleration, W the thickness of the rectangular reservoir perpendicular to flow, and λ_{rt}^m the total relative mobility in the mixed zone. The volumetric sweep increases with increasing L_g or R_g, which depend on the total injection rate Q_t.

Shi and Rossen (1998) declared that the only way to control gravity segregation is to increase injection-well pressure when the steady injection is performed into a given reservoir. They also discussed the implications of this model for field application of foams. Rossen and Van Duijn (2004) proved that Eqs. 1 and 2 are rigorously correct as long as the standard assumptions of fractional-flow theory are applied. Rossen and Shen (2007) explicitly showed the relation between injection-well pressure and segregation length. Rossen and Stolwijk (2009) found that these two equations are reasonably accurate for heterogeneous reservoirs with small degrees of heterogeneity, such as mildly heterogeneous layered or checkerboard reservoirs, if one adjusts the vertical permeability to account for the heterogeneity. However, when heterogeneity is more severe, L_g is not a good measure of sweep efficiency. Rossen et al. (2010) proved that this model can be extended to foam flow as long as injection is uniform along the wells, despite the complexity of foam behaviour.

Stone's model is extended to dipping reservoirs based on numerical simulations (Jamshidnezhad, 2009; Yu et al., 2017) or derivation of an analytical model where some assumptions are not rigorously accurate (Jamshidnezhad and Ghazvian, 2011; Namani et al., 2012; Khan and Mandal, 2020). As per our knowledge, until now, there have been few studies to investigate the gravity segregation in the foam-EOR process, especially considering reservoir heterogeneity. In this work, we investigate the effect of reservoir heterogeneity on gravity segregation in foam-EOR processes. An implicit-texture (IT) model (CMG-STARS, 2012) called the 'STARS' model, used in this study, assumes that foam generation and destruction reach a local steady-state instantaneously and represents the effect of foam bubbles implicitly by introducing a mobility-reduction factor. This mobility-reduction factor, used to rescale gas mobility with foam, is a function of water saturation, oil saturation, surfactant concentration, capillary number, and salinity. For simplicity, we assume that oil is absent in our model and surfactant is already present in the water phase throughout the porous medium. The foam model we use is shown in Appendix.

In order to accurately simulate these highly nonlinear foam EOR processes, a new approach, named Operator-Based Linearization (OBL), where performance, flexibility, and robustness can be combined, was introduced to reduce the nonlinearity of complex physical problems (Khait and Voskov, 2018). The OBL approach transforms the discretized mass-conservation equations into space-dependent and state-dependent operators. The state-dependent operators are approximated by a discrete representation on a uniform/nonuniform mesh in parameter space. These state-dependent operators rely on current local physical properties (e.g. density, viscosity, relative permeability), which represent the most nonlinear part of governing equations. The continuous representation of these operators is achieved through multilinear interpolation, which provides a unique tool for approximate representation of the exact physics of the problem. The OBL approach also provides an opportunity to control the nonlinearity in physics by changing the resolution of parameter space.

The paper is structured as follows. First, we briefly describe our numerical model and OBL approach. Next, we validate the simulation by comparing numerical results with analytical solutions. Then, we investigate the effect of permeability and reservoir heterogeneity on gravity segregation. We end the paper up with a discussion and summary of main conclusions.

Model description

Mathematical model

In this section, we briefly consider the governing equations and nonlinear formulation for two-phase, two-component isothermal foam simulation through porous media. These equations describe the conservation of mass in a foam system with n_p phases and n_c components:

$$\frac{\partial}{\partial t}(\phi \sum_{j=1}^{n_p} x_{cj}\rho_j s_j) + div \sum_{j=1}^{n_p} x_{cj}\rho_j \mathbf{u}_j + \sum_{j=1}^{n_p} x_{cj}\rho_j \widetilde{q}_j = 0, \qquad c = 1,2\cdots,n_c, \tag{3}$$

where j is the corresponding phases (gas and water), ϕ is porosity, s_j is phase saturation, ρ_j is phase molar density, x_{cj} is component mole fraction in a phase, u_j is the velocity of each phases, q_j is the volume flow rate of each phase due to source and sink.

The saturation constraint requires

$$\sum_{j=1}^{n_p} s_j = 1. \tag{4}$$

In addition, Darcy's law is applied to describe the flow of each phase:

$$\mathbf{u}_j = -K\frac{k_{rj}}{\mu_j}(\nabla p_j - \rho_j g \nabla D), \tag{5}$$

where K is permeability tensor, k_{rj} is relative permeability, u_j is phase viscosity, p_j is phase pressure, g is the gravitational acceleration, and D is the depth.

A finite-volume discretization on a general structured mesh and backward Euler approximation in time is applied. This introduces strong nonlinearity into the system of the governing equations. We need to linearize the problem, and the Newton-Raphson method is adopted to solve the linearized system of equations on each nonlinear iteration. In the conventional simulation, the Jacobian should be assembled with accurate numerical property values and their derivatives with respect to nonlinear unknowns. This process requires either various interpolations (for properties such as relative permeabilities of different phases) or solution of a highly nonlinear system in combination with chain rule and inverse theorem, which could increase the computational cost.

OBL approach

Following the OBL approach, all variables in the Eq. 3 fully defined by the physical state ω can be grouped together and represented by the state-dependent operators (Khait and Voskov, 2017; Voskov, 2017). Taking into account buoyancy, the discretized mass-conservation equation in operator form is

$$V\phi_0[\alpha_c(\omega) - \alpha_c(\omega_n)] + \sum_{l\in L(i)}\sum_{j}^{n_p} \Delta t \Gamma^l \beta_{cj}^l(\omega)(\Delta p_j^l - \rho_{j,ave}^l g \Delta D^l) + \theta(\xi,\omega,u) = 0, \tag{6}$$

where

$$\alpha_c(\omega) = (1 + c_r(p - p_{ref}))\sum_{j=1}^{n_p} x_{cj}\rho_j s_j, \tag{7}$$

$$\beta_{cj}(\omega) = x_{cj}\rho_j k_{rj}/\mu_j, \tag{8}$$

$$\gamma_j(\omega) = \rho_j g, \tag{9}$$

$$\theta(\xi,\omega,u) = \Delta t \sum_{j=1}^{n_p} x_{cj}\rho_j q_j(\xi,\omega,u), \tag{10}$$

where ω and ω_n are nonlinear unknowns in the current and previous timestep, respectively; $L(i)$ is the set of neighbors of the control volume l; and $\theta(\xi,\omega,u)$ is the source term. V, ϕ_0, and c_r are initial volume, porosity and rock compressibility respectively, which represent the reservoir rock properties. ρ_j, k_{rj}, and μ_j, are phase density, phase relative permeability and phase viscosity, respectively. Γ^l is a constant geometrical part of transmissibility, combining absolute permeabilities and geometries of neighboring control volumes. Here, the phase-potential-upwinding (PPU) strategy, where phase mobilities are selected based on the phase potential difference, is applied to compute the numerical flux. The details can be found in Khait and Voskov (2018).

Comparison with the analytical model

To calibrate our simulator, we first compare numerical results with the analytical model for a horizontal homogeneous reservoir with different injected water fractions in the presence and absence of foam. For this study, a 2D horizontal rectangular grid is constructed and the size of grid block is 1×1×1 m. The parameter settings, such as permeability and foam parameters, are listed in Table 1. For a

better resolution, the permeability of the foam-injection model is 10 times higher than that without foam. The relative-permeability model is shown in Appendix. The top and the bottom surfaces of the reservoir are no-flow boundaries. The injection wells (with fixed total injection rate of 1.5 m^3/day at reservoir condition) and one production well (fixed bottom hole pressure at 138 bar) are located at the left boundary and right boundary, respectively, perforating all layers in the vertical direction. In this study, we run simulations with separate injection wells in each grid block with a fixed injection rate and f_w in each well to ensure f_w^J is exactly uniform along the entire length of the reservoir. Such a small injection rate is chosen so that segregation would occur within the reservoir volume. We assume the reservoir is isotropic; the horizontal permeability is equal to the vertical permeability. Capillary pressure is neglected in this study. From Stone (1982) and Jenkins (1984), one pore volume (PV) of gas should be sufficient to reach steady state. So in our simulation, 2 PV of gas is injected to ensure that the injected gas and water can be segregated completely. We test eight cases with different injected water fractions of 5%, 10%, 15%, 20%, 25%, 30%, 35% and 40%.

Table 1 *Parameter settings used in 2D horizontal models*

	Reservoir dimension	Permeability, mD	Porosity	Foam parameters		
				fmmob	*fmdry*	*epdry*
No foam	100×1×30	50	0.2	-	-	-
Foam	400×1×30	500		3400	0.13	10000

Fig. 2 shows the water-saturation profile without and with foam at steady state for uniform co-injection of gas and water (f_w = 20%) along the entire vertical interval. There are a mixed zone of nearly homogeneous saturation, an underride zone of uniform saturation (S_w = 1), and a steady-state override zone with water at its residual saturation. There are some visible differences if foam is injected. First, in the mixed zone, the water saturation with foam injection is much lower than that without foam, in order to accommodate the same fractional-flow of water. Foam can significantly reduce gas mobility; the reduction of gas mobility by foam causes the injection pressure to increase if the injection rate is fixed. The second difference is the segregation length. With the same conditions except the absolute permeability, when foam is injected, the segregation length increases by over two orders of magnitude compared to that without foam. Eq. 1 predicts that the reduction of the total mobility in the mixed zone with foam mitigates the effect of gravity segregation at the price of increased injection pressure.

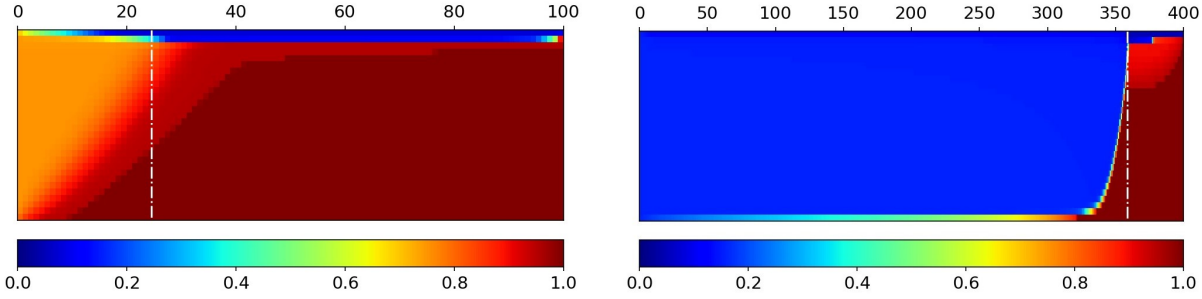

(a) No foam (b) Foam injection

Figure 2 *Water saturation profile (f_w = 20%) at steady state. The white dashed line is the segregation point predicted by Eq. 1. In both cases, there are transition zones where water saturation is lower than initial condition.*

Fig. 3 compares the segregation length with and without foam between the analytical solutions and numerical solutions. In Fig. 3(a), we show the ultimate segregation length with and without the transition zone. As predicted by Stone's model, the water saturation is uniform at a saturation $S_{w,mix}$ in the mixed zone. To minimize the effect of numerical dispersion, we distinguish the mixed zone where the water saturation is equal to or smaller than ($S_{w,mix} + 0.001$). Numerical dispersion plays a significant role in the segregation length for the case without foam, as shown in Fig. 3(a), because of its effect on mobility in the mixed zone. Fig. 3(b) shows that foam quality significantly affects the segregation length by modifying the total relative mobility of the mixed zone in Eq. (1). In the high-quality regime, the

segregation length increases with decreasing foam-quality; on the contrary, it decreases when foam-quality decreases in the low-quality regime. The segregation length approaches a maximum value in the transition between the two regimes, where the foam apparent viscosity is highest, i.e., lowest total relative mobility. The distance of complete gravity segregation agrees with the analytical solutions quite well. Excluding the effect of numerical dispersion, our numerical model shows good agreement with analytical solutions predicted by Stone (1982) and Jenkins (1984).

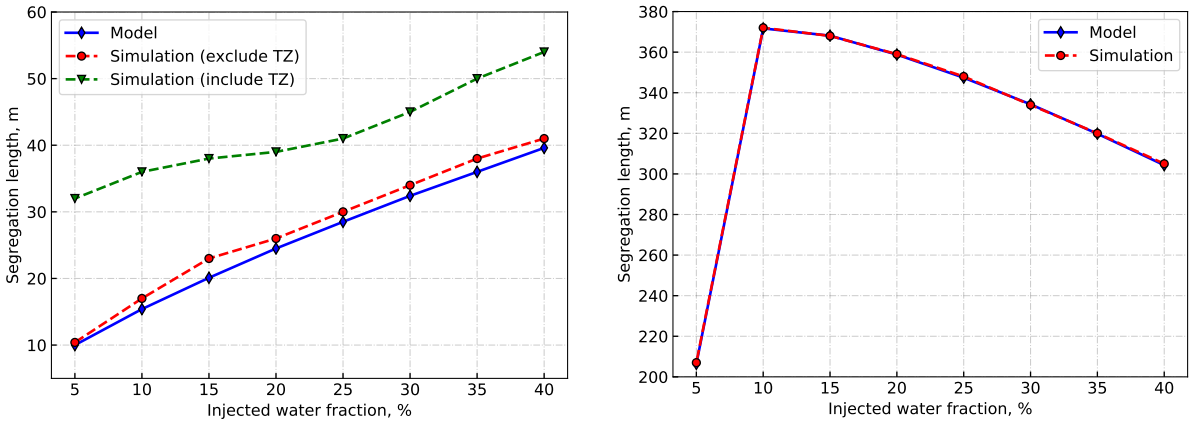

(a) No foam

(b) Foam injection

Figure 3 *Comparison between analytical model and simulation results. (a) no foam; (b) foam. 'TZ' is an abbreviation of 'Transition Zone'.*

Numerical dispersion study

Both cases show a dispersed zone along the boundaries, and this zone is extended a few grid blocks in the simulation (Fig. 2) in part due to the numerical dispersion and in part due to the lower gas mobility during the period of two-phase transient displacement (Stone, 2004; Rossen and Stolwijk, 2009; Rossen et al., 2010; Yu et al., 2017). These transition zones are not included in Stone's model because this model is a static model designed to depict a steady state. Stone notes that numerical dispersion plays an important role and is difficult to control in the course of simulation of these processes. In this section, the effect of numerical dispersion on gravity segregation is discussed in terms of grid size for the case where gas and water are co-injected with f_g = 80% and only gas is injected with f_g = 100%. We ignore the influence of time-step and OBL resolution. Then we quantitatively evaluate the differences between the analytical and numerical solutions.

At first, we use a simple 1D model to investigate the effect of numerical dispersion in the presence and absence of foam with different f_g by comparing to analytical solutions. Fractional-flow theory is applied to provide analytical solutions (Zhou et al., 1995). The corresponding fractional-flow curves for gas-water and foam system are show in Fig. 4. Here a 1D homogeneous porous medium with 1000 grid blocks (grid size is 0.1m) is constructed. In all tests, the total injection rate (0.05 m^3/day) is fixed with a value of f_g of 80% and 100%, respectively.

Fig. 5 shows the total-relative-mobility and gas-saturation profiles after 0.2 PVI with f_g = 80% (J_f and J_{gw} in Fig. 4). With foam injection (J_f), the total relative mobility is reduced significantly behind the leading edge of the gas bank; the gas saturation thus increases. With the same injected gas fraction, the whole path of foam injection disappears into the shock (analytical), while the shock is followed by a spreading wave if the foam is absent (see Fig. 5(a) and Fig. 4). The numerical solutions show good agreement with analytical solutions, except for small deviations without foam (Fig. 5(a)) which can be eliminated by increasing the grid resolution. These two cases can represent the advance of the mixed zone, as shown in Fig. 2.

Fig. 6 shows the total-relative-mobility and gas-saturation profiles after 0.2 PVI with f_g = 100% (J_g in Fig. 4). In these two cases, during gas injection, there is a spreading wave behind the shock front. The

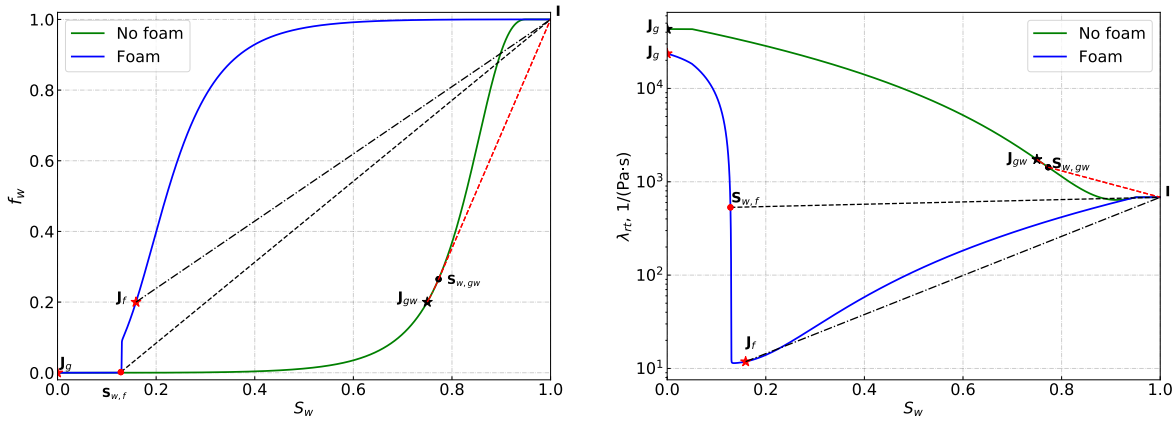

(a) Water fractional flow curves (b) Total relative mobility curves

Figure 4 *Water fractional flow and total-relative-mobility curves without and with foam. The dashed lines connect the initial condition (f_w=1) and shock position at leading edge of gas bank (dotted point). I is the initial condition, J_g is the gas injection condition (f_g=1), and J_f and J_{gw} are foam injection and gas-water co-injection with f_g of 80%, respectively. $S_{w,f}$ and $S_{w,gw}$ are the shock positions with and without foam, respectively. In the presence of foam, there is a big jump at the shock at leading edge of gas bank; during gas injection, all saturations between S_w = 1 and the leading edge of the shock disappear into the shock.*

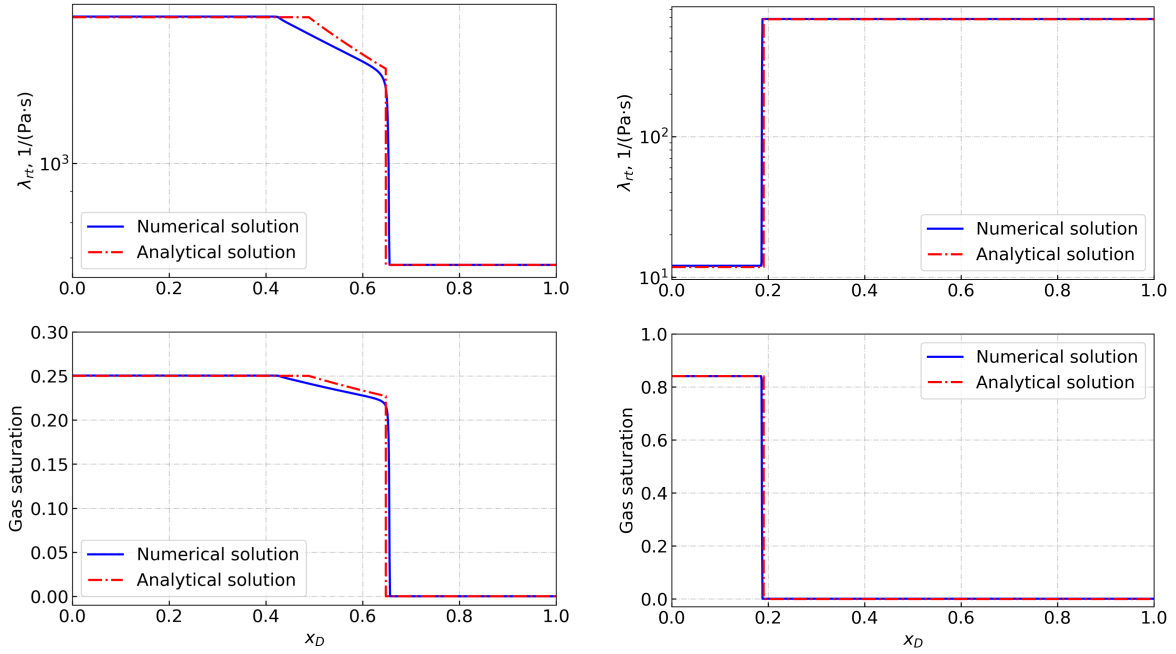

(a) No foam (b) Foam injection

Figure 5 *Total relative mobility and gas saturation profiles with f_g=80% after 0.2 PVI without and with foam injection. The top figure is total relative mobility profile, and the bottom one is the gas saturation profile. These two cases can represent the displacement in the mixed zone.*

numerical solutions show good agreement with analytical solutions except the shock front. Because numerical simulations do not represent shocks well, the numerical total relative mobility is smaller, with an intermediate saturation in at least one grid block with intermediate saturation between the two banks. In the presence of foam, there is a low-mobility zone behind the shock front, a high-gas-mobility zone near the well, and at least one gridblock with extraordinarily low mobility behind the shock front (Fig. 6(b)). This low mobility in the spreading wave behind the shock causes the large transition zone

between override- and underride-zone in the presence of foam, as shown in Fig. 2(b).

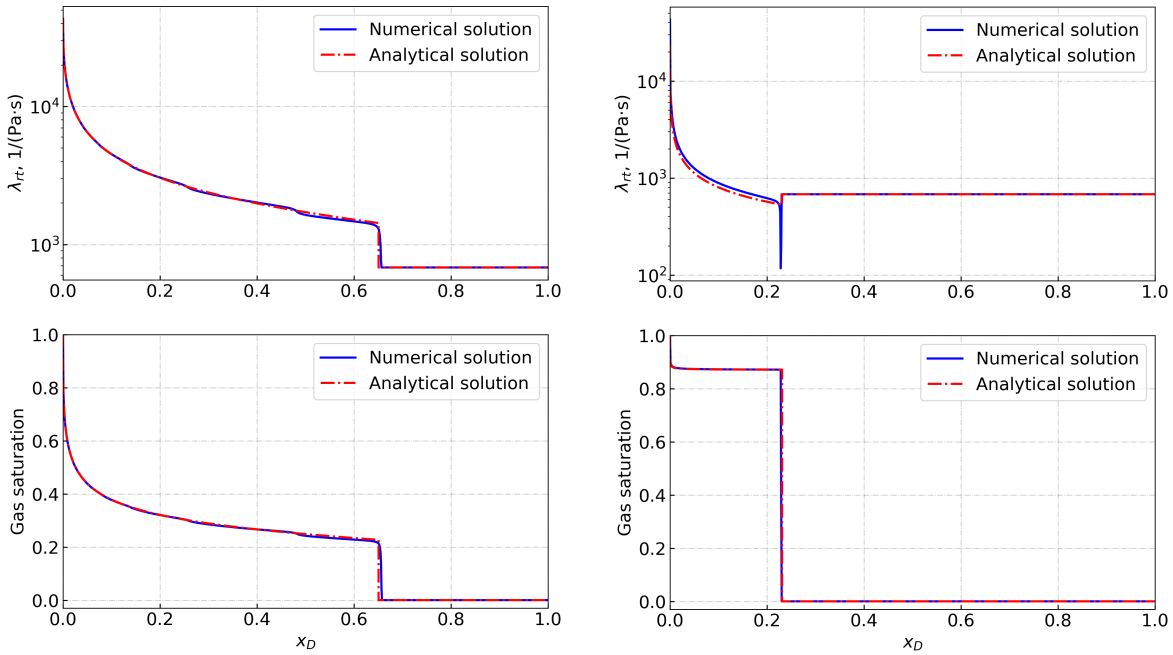

(a) No foam (b) Foam injection

Figure 6 *Total relative mobility and gas saturation profiles with f_g=100% after 0.2 PVI without and with foam injection. The top figure is total relative mobility profile, and the bottom one is the gas saturation profile. These two cases can represent the displacement in the override zone.*

To verify the causes of transition zones in Fig. 2, we then run several small 2D models to investigate the effect of grid resolution. For a better resolution, without foam injection, the size of the domain is 40 m × 1 m × 20 m, with different size of grid block (0.1 m × 1.0 m × 0.1 m, 0.5 m × 1.0 m × 0.5 m and 1.0 m × 1.0 m × 1.0 m); in the presence of foam, the size of the domain is 500 m × 1 m × 30 m with grid block size of 1.0 m × 1.0 m × 0.5 m and 1.0 m × 1.0 m × 1.0 m, respectively. We find that the transition zone between the mixed and underride zones is insignificant when foam is present. We therefore only change dz to check the effect of grid size on the transition zone beneath the override zone. The injected f_g is fixed at 0.8 in all cases.

According to Jenkins's model (Jenkins, 1984), the thickness of over-/under-ride zone at steady-state can be determined by:

$$\frac{H_w}{H_g} = WAG\frac{\lambda_{gg}}{\lambda_{ww}} = \frac{Q_w}{Q_g}\frac{\lambda_{gg}}{\lambda_{ww}} \tag{11}$$

where H_w and H_g are the thickness of override zone and underride zone, and λ_{gg} and λ_{ww} are the gas relative mobility in override zone and water relative mobility in underride zone, respectively. Specifically, Jenkins (1984) assumes that λ_{gg} is gas mobility at irreducible water saturation, and λ_{ww} is water mobility at 100% water saturation. WAG ratio is determined by water volumetric injection rate Q_w and gas volumetric injection rate Q_g.

Fig. 7 shows gas saturation (no foam injection) at steady state with different grid sizes. The segregation length differs among the cases due to the change of grid resolution. There is a transition zone existing at the boundary between the mixed and underride zones. Below the override zone, there is another region where gas is not expected to be present in the model. The height of the override zone is around 1.2 m from Eq. 11. With size dz = 1.0 m, there is a large deviation in either segregation point or the thickness of the override zone from the analytical result. With a finer grid, this transition shrinks but still appears. When the grid block size is 0.1 m, the differences between the analytical solutions and numerical solutions are insignificant, as shown in Fig. 7(a). We can infer that the transition zones

between regions are caused by numerical dispersion when the foam is absent. By increasing the grid resolution, the numerical solutions are close to analytical solutions, but the computational cost, in turn, increases.

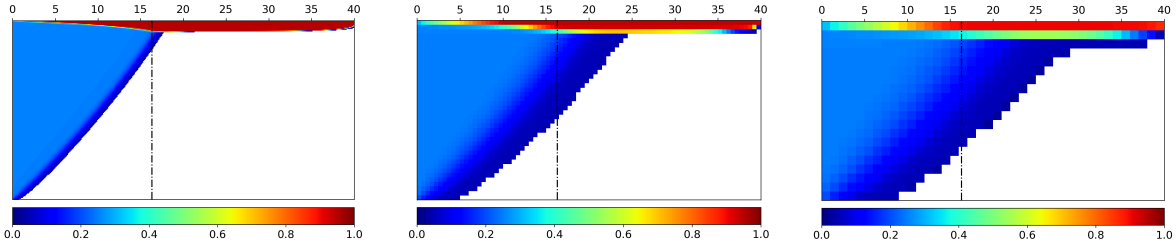

(a) $(dx, dz) = (0.1, 0.1)$ m (b) $(dx, dz) = (0.5, 0.5)$ m (c) $(dx, dz) = (1.0, 1.0)$ m

Figure 7 *Gas saturation profile (no foam) at steady state with different grid size. In a region with white color, gas saturation is less than residual gas saturation. The black dashed line is the segregation point predicted by Eq. 1.*

Fig. 8 shows gas saturation (with foam injection) after 2.0 PV gas injection with different grid sizes. The transition zone between the mixed zone and the underride zone is negligible. Once foam is injected into the formation, the gas mobility is reduced significantly. Each grid block travels through saturations from injection condition (shock) to initial condition, as shown in Fig. 5(b). At all these saturations, total mobility is intermediate between that at the initial and injected saturations (Fig. 4(b)). In the override zone ahead of foam, gas migrates to upper layers and accumulates there . Foam therefore is weaker and weaker until foam collapses completely in the override zone. In this process, all grid blocks in the override zone have to travel through saturations of extremely low mobility (Fig. 4(b); Fig. 6(b)), thus much gas is diverted into the underride zone. This process is not represented in Stone's model. After steady-state, there is a thick transition region between the override and underride zones. This effect does not disappear with grid refinement. It is a real effect caused by the low mobility in the spreading wave behind the shock (Rossen, 2013).

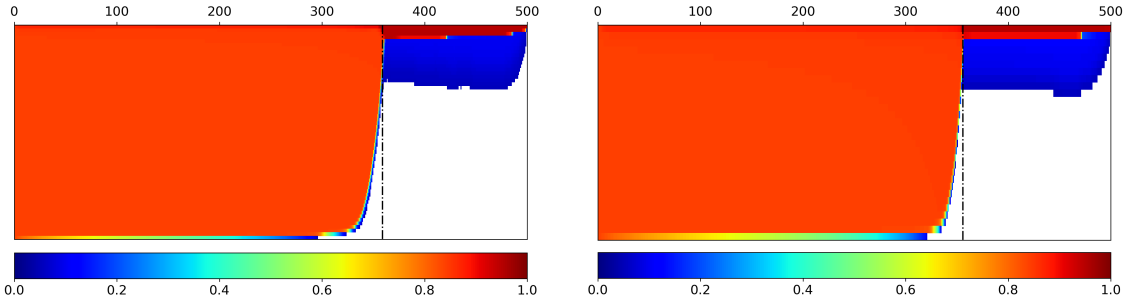

(a) $(dx, dz) = (1.0, 0.5)$ m (b) $(dx, dz) = (1.0, 1.0)$ m

Figure 8 *Gas saturation profile (foam injection) at steady state with different grid size. In a region with white color, gas saturation is less than residual gas saturation. The black dashed line is the segregation point predicted by Eq. (1).*

Gravity segregation in heterogeneous porous media

In this study, we represent heterogeneity using foam parameters by fitting the foam-quality scans from Moradi-Araghi et al. (1997). They tested the effect of rock permeability on CO_2-foam strength. The permeability of the reservoir formations they tested ranges from 32.8 to 551.5 mD. In order to extract foam model parameters from their experimental data, we assume that the permeability does not change the rock wetting behaviour: Corey exponents and residual saturations in water-gas relative-permeabilities are the same in the different formations. In our simulation, a rectangular reservoir is used to simulate the gravity-segregation process. We neglect shear-thinning in the low-quality regime. Based on these assumptions, we fit the foam parameters for the STARS model.

The relative-permeability data and foam parameters are listed in Table 2. Fig. 9 presents the gas apparent viscosity as a function of foam quality for rocks with different permeabilities. As is shown, two regimes can be observed for all permeabilities: the apparent viscosity of foam increases and reaches a maximum value with increasing foam quality (low-quality regime) and thereafter decreases with further increase in foam quality (high-quality regime). Moreover, the foam apparent viscosity increases with increasing permeability, i.e., foam appears to be stronger in rock with higher permeability.

Table 2 *Corey relative-permeability parameters and foam parameters fit to coreflood data for formations with different permeability from Moradi-Araghi et al. (1997).*

	Permeability, mD	k^0_{rw}	n_w	k^0_{rg}	n_g	S_{wc}	S_{gr}	$fmmob$	$epdry$	$fmdry$
K_1	32.8	0.2	2.0	1.0	1.8	0.1	0.05	1.02×10^3	2.50×10^4	0.185
K_2	56.8							1.58×10^3	9.40×10^3	0.171
K_3	169.8							3.14×10^3	6.96×10^3	0.155
K_4	551.5							9.74×10^3	4.76×10^3	0.136

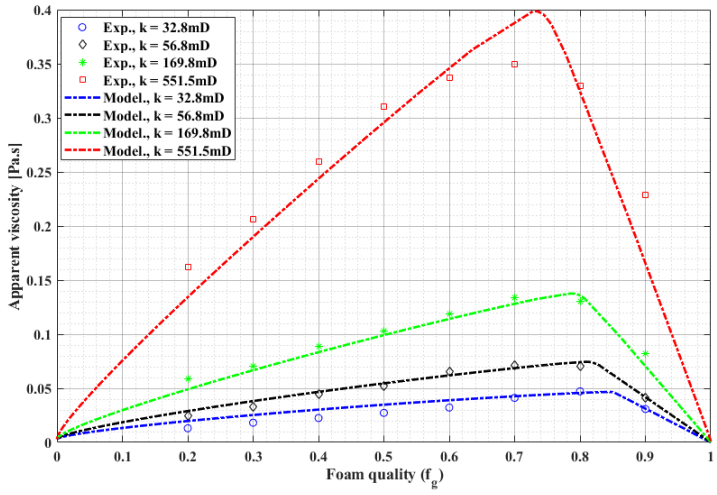

Figure 9 *Fit of the model to experimental data.*

Effect of permeability in homogeneous reservoirs

In this section, we investigate the effect of permeability on gravity segregation in the presence of foam using the parameters in Table 2. The dimension of the domain is 200 × 1 × 30 m with gridblock size of 1 m × 1 m × 1 m. Due to the mobility reduction in the presence of foam, the magnitude of the segregation length predicted by Eq. (1) is of order 10^3 m for all four permeabilities if the total injection rate along the entire vertical interval is 1.5 m^3/day, with f_w = 15%. In practice, the distance between an injector and a producer is usually shorter. Therefore, in this and following simulation results (except where noted), the injection rate is reduced to 0.15 m^3/day, with f_w = 15%, for better resolution of foam behaviour in a reasonable distance. In all cases, 2.35 PV (corresponding to 2.0 PV of gas) injection is sufficient to achieve steady state.

Under the same injection conditions, the segregation length in different formations is different, as shown in Fig. 10. In the higher-permeability formation with K = 551.5 mD, gas and water separate with each other in a relatively short distance; the segregation length is longer in the lowest-permeability case, approximately 160 m. With a fixed total injection rate, the segregation length increases with decreasing permeability, as predicted by Eq. 1. Because apparent viscosity increases with increasing permeability (Fig. 9), the increase in segregation length is relatively small. Water saturation in the mixed zone is close to the limiting water saturation ($fmdry$ in the IT model) in all cases.

Fig. 11 illustrates the relationship between the segregation length (or apparent viscosity) and permeabil-

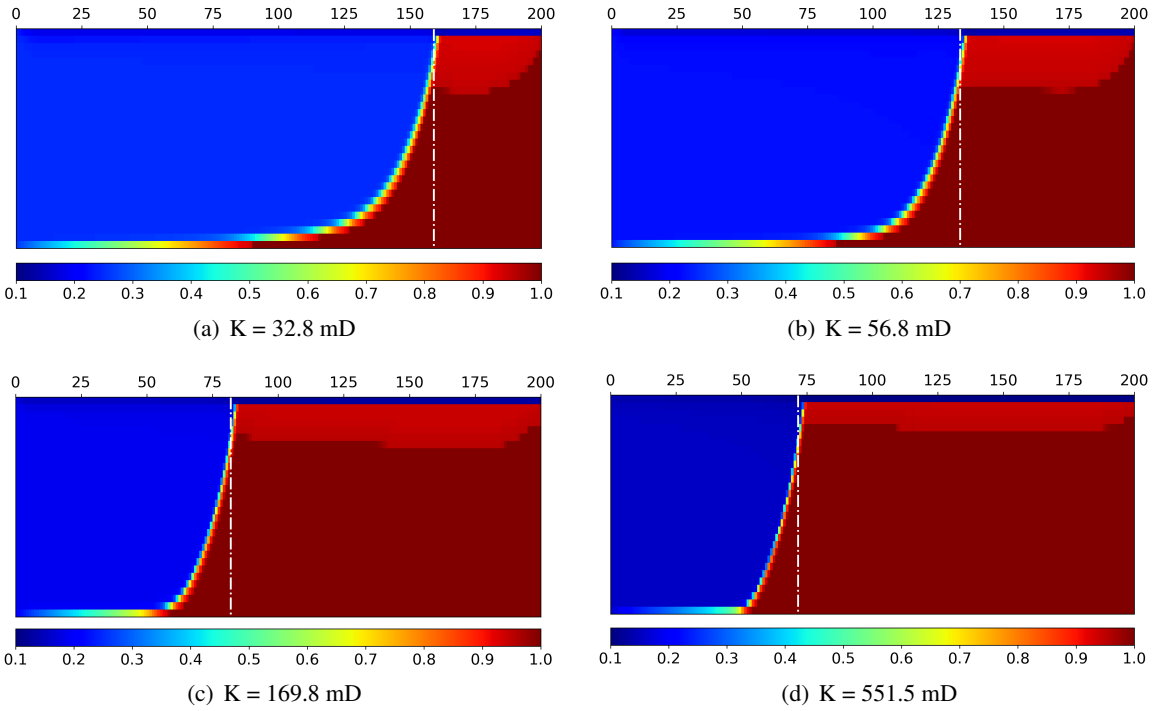

(a) K = 32.8 mD (b) K = 56.8 mD

(c) K = 169.8 mD (d) K = 551.5 mD

Figure 10 *Water-saturation profiles at steady state in formations with different permeabilities. The white dashed line is the segregation point predicted by Eq. 1.*

ity. Foam is stronger (higher apparent viscosity) in the higher-permeability formation where the limiting capillary pressure is lower, as shown in Fig. 11(a). The segregation length, however, decreases with the increase of permeability. From Eq. 1, the segregation length depends on the combination of vertical permeability and total relative mobility (i.e., apparent viscosity) in the mixed zone if the total injection rate is fixed in a given grid. Fig. 11(b) shows the variation of segregation length with the permeability and apparent viscosity in the mixed zone. The segregation length decreases with the increase in $(K/\mu_{app}) = (K_z\lambda_{rt})$. Under the same injection condition, the low-permeability formation gives a longer segregation length, as predicted by Eq. 1. In our study, we only have these four sandstone formations available with limited physics. More studies should be carried out to investigate the effect of permeability on foam strength and segregation length.

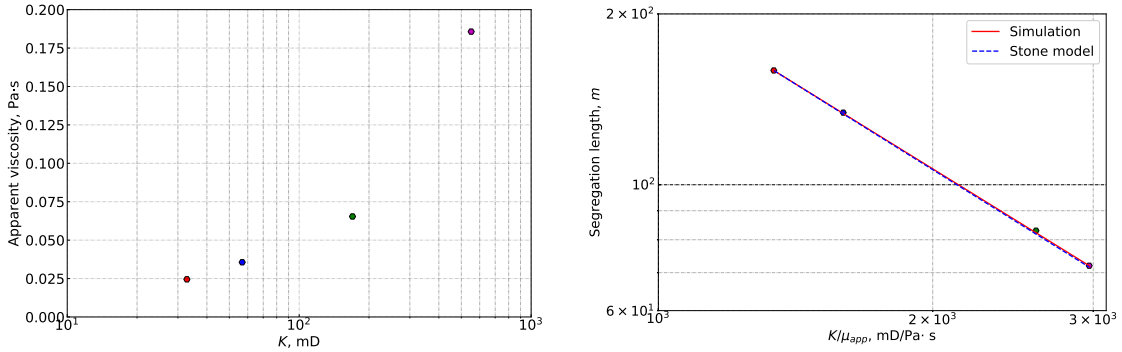

(a) μ_{app} vs. K (b) L_g vs. K/μ_{app} $(= K_z\lambda_{rt})$

Figure 11 *The relationship between segregation length (or apparent viscosity) and permeability. (a) The absolute permeability is plotted in the logarithmic space; (b) In log-log space, the segregation length is a linear function of $(K/\mu_{app}) = (K_z\lambda_{rt})$: the simulation results agree with Stone's prediction.*

Effect of reservoir heterogeneity: two-layer case

Reservoir heterogeneity influences sweep efficiency and thus recovery. Stone (1982) demonstrated that barriers to vertical flow, such as a low-permeability zone, can give an incremental recovery compared to a homogeneous reservoir. In this part, we study the effect of reservoir heterogeneity on gravity segregation during a foam EOR process in a two-layer reservoir, as shown in Fig. 12, with different layer permeabilities, thickness, and foam parameters. The total thickness keeps constant (30 m), but the layer thickness can be varied based on different thickness ratios. The permeabilities (K_1 = 32.8 mD, K_2 = 56.8 mD, K_3 = 169.8 mD, and K_4 = 551.5 mD) and the corresponding foam parameters are shown in Table 2. The total injection rate is fixed at 0.15 m^3/day with foam quality f_g of 85% in all cases. We assume for this study that there is no barrier to flow between the layers.

To keep the injection pressure uniform along the entire length of the reservoir (left boundary), the total injection rate is split into two streams based on total mobility in the mixed zone and thickness ratio between two layers. Each injection well in each gridblock is fixed with a injection rate by averaging the corresponding stream in that layer. For comparison, we use two homogeneous models to calculate the segregation length as references. These two homogeneous models are the same as the two-layer model, such as total injection rate, total thickness, and foam quality, except for the uniform permeability which is equal to the permeability of either the top layer or the bottom layer.

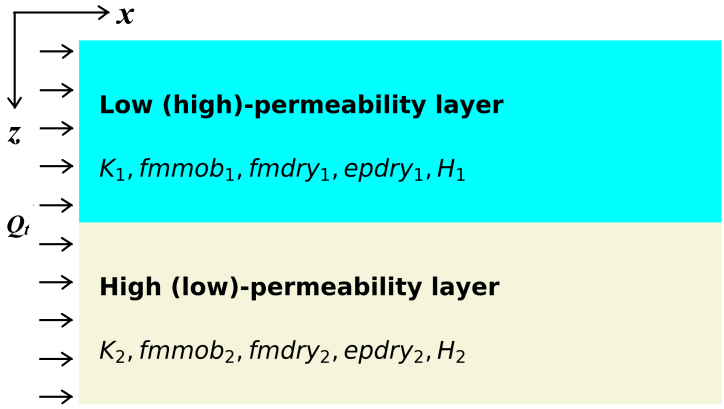

Figure 12 *Schematic of the 2D layer-parallel flow model used in this work. In each layer, the thickness (H), permeability (K), and foam parameters (fmmob, fmdry, epdry) are different. For different permeability ratios, the thickness of each layer is also varied, depending on the thickness ratio. The corresponding foam parameters can be found in Table 2.*

A dimensionless parameter Ω is defined as

$$\Omega = \frac{L_{g,r} - L_{g,H}}{L_{g,L} - L_{g,H}}, \tag{12}$$

where $L_{g,r}$, $L_{g,H}$ and $L_{g,L}$ are segregation length in two-layer model, single-layer model with higher permeability and single-layer model with lower permeability, respectively. The single-layer model keeps same conditions as the two-layer model except for the permeability. This parameter Ω can be used to evaluate the effect of the low-permeability layer on the ultimate segregation length of a two-layer system. Ω approaching 1.0 means the segregation length of the two-layer model is dominated by the low-permeability layer; otherwise, if Ω is close to 0.0, the high-permeability layer plays a more important role.

Fig. 13 shows the variation of segregation length with different permeability ratios and thickness ratios. If the lower-permeability layer is at the bottom, Ω decreases with the increasing thickness ratio: the lower-permeability layer on the bottom dominates. Once the thickness ratio is above a certain value, Ω does not change with thickness ratios, approaching to 0, as shown in Fig. 13(a). The thickness ratio is around 0.5 in cases where the high-permeability layer is on the top: i.e., the segregation length is

completely dominated by the higher-permeability layer if the height of higher-permeability layer (top) is more than half of that of the low-permeability layer (bottom). The curves with different permeability ratios almost overlap together, which indicates that Ω follows the same trend when the higher-permeability layer is on the top regardless of permeability contrast. In contrast, Ω increases with the increasing thickness ratio and approaches 1 if the lower-permeability layer is on the top (Fig. 13(b)). However, there is a wide spread in results among the cases. When the permeability contrast is larger (i.e., smaller ratio), the required thickness ratio for a constant segregation length increases; the effect of the higher-permeability layer at the bottom is more significant.

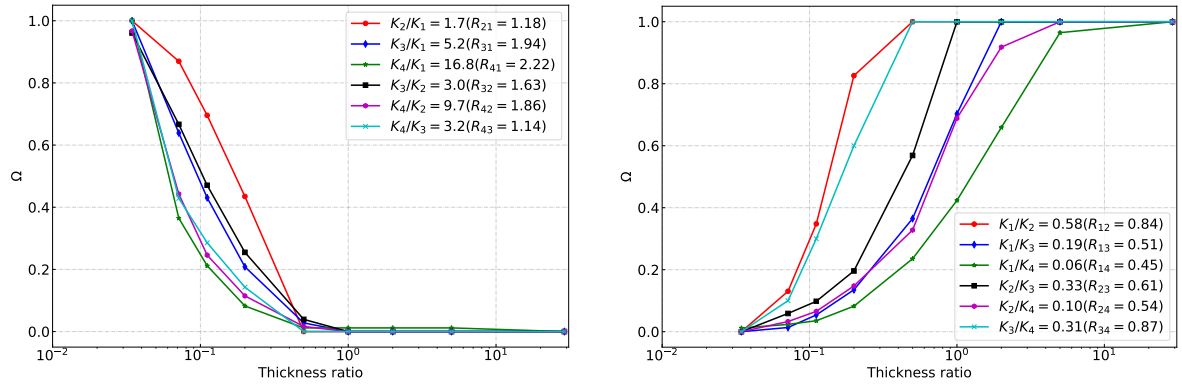

(a) Higher perm. on top

(b) Lower perm. on top

Figure 13 *Gravity-segregation point changes with different permeability ratios and thickness ratios. In both cases, K_1<K_2<K_3<K_4. The higher-permeability is on the top in (a), and is at the bottom in (b). The thickness ratio is defined as H_{top}/H_{bottom}. R_{ij} is the ratio of total mobility in the two layers.*

Fig. 14 shows the effects of permeability ratio and thickness ratio on total mobility distribution and segregation distance at steady-state in cases where the higher-permeability layer is on the top. With a smaller thickness ratio (see the left column in Fig. 14), the amount of gas in the high-permeability layer does not affect segregation in the lower-permeability layer (bottom). Foam is stronger in the high-permeability layer, corresponding to a higher apparent viscosity (see Fig. 9), which limits the effect of the high-permeability layer on gravity segregation. With increasing thickness of the high-permeability layer, the top layer starts to dominate the segregation process. The segregation occurs earlier in the top layer due to higher total mobility. Once gas and water segregate completely, the gas in the lower-permeability layer at the bottom cannot propagate further.

Conclusions

In this study, we extend the OBL approach to investigate gravity segregation with foam in heterogeneous reservoirs. The following conclusions can be drawn:

- The numerical results show good agreement with analytical solutions in horizontal homogeneous reservoirs in the presence and absence of foam. Through fractional-flow theory, we find that the transition zone during water-gas co-injection is caused by numerical dispersion. The transition zone beneath the override zone with foam injection is not a numerical artefact, but caused by the low gas relative-mobility during the transient displacement process.
- Permeability affects both the mobility reduction of wet foam in the low-quality regime and the limiting capillary pressure at which foam collapses. With a fixed injection rate, the segregation length depends on the combination of vertical permeability and foam apparent viscosity (i.e., total mobility).
- Reservoir heterogeneity plays an important role in gravity segregation. In two-layer models, the thickness of the top layer plays an important role in the ultimate segregation length. A thin top

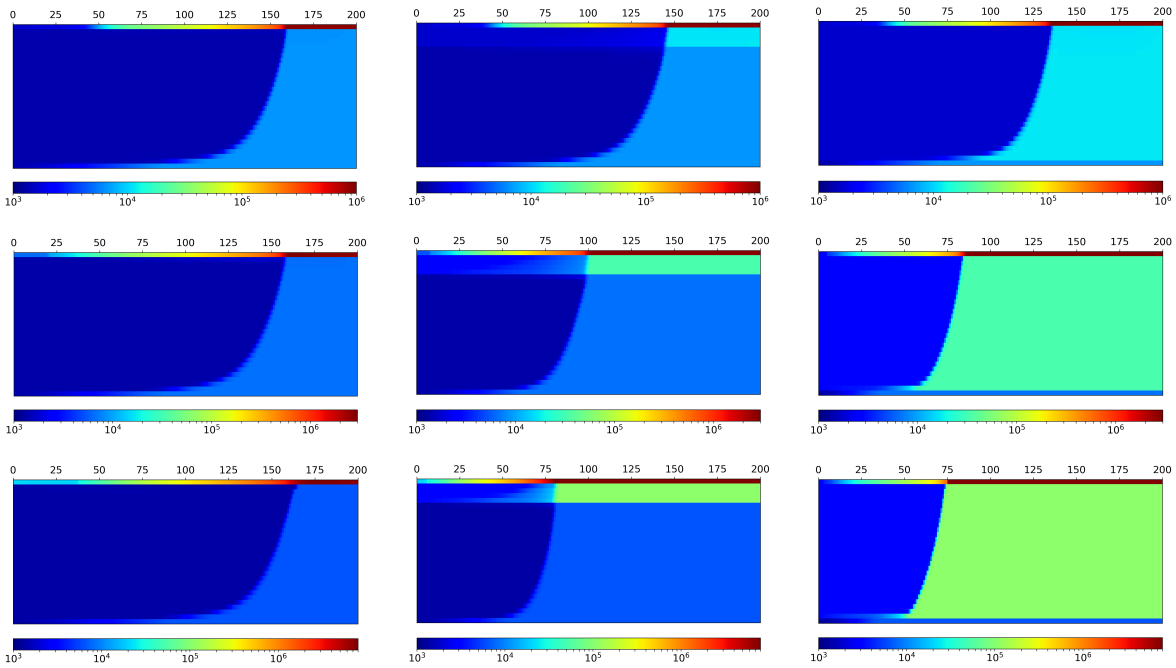

Figure 14 *Total mobility $(mD/(Pa \cdot s))$ distributions in different layers at steady state. In all case, the lower-permeability layer is at the bottom. The plots illustrate different permeability ratios $\left(K_2/K_1$ (first row), K_3/K_1 (second row), and K_4/K_1 (last row)$\right)$ and different thickness ratios $\left(1$ m/29 m (first column), 5 m/25 m (second column), and 29 m/1 m (last column)$\right)$, respectively.*

layer does not affect segregation in the bottom layer, while a thicker top layer dominates the segregation length, with less influence of the bottom layer.

During foam injection, surfactant could lag the gas depending on injected quality and adsorption. Geologically, heterogeneity is more complex than represented here; that complexity would of cause affect the gravity segregation process. These factors are neglected in this research but remain a future research priority.

Acknowledgements

We acknowledge the financial support of China Scholarship Council (No.201706440023).

References

Cheng, L., Reme, A., Shan, D., Coombe, D. and Rossen, W. [2000] Simulating foam processes at high and low foam qualities. In: *SPE/DOE improved oil recovery symposium*. Society of Petroleum Engineers.

CMG-STARS [2012] Computer Modeling Group Ltd. *Calgary, AB, Canada*.

Dholkawala, Z.F., Sarma, H. and Kam, S. [2007] Application of fractional flow theory to foams in porous media. *Journal of Petroleum Science and Engineering*, **57**(1-2), 152–165.

Jamshidnezhad, M. [2009] Gravity segregation in gas improved oil recovery of tilted reservoirs. In: *EUROPEC/EAGE Conference and Exhibition*. Society of Petroleum Engineers.

Jamshidnezhad, M. and Ghazvian, T. [2011] Analytical modeling for gravity segregation in gas improved oil recovery of tilted reservoirs. *Transport in porous media*, **86**(3), 695–704.

Jenkins, M. [1984] An analytical model for water/gas miscible displacements. In: *SPE enhanced oil recovery symposium*. Society of Petroleum Engineers.

Khait, M. and Voskov, D. [2018] Adaptive parameterization for solving of thermal/compositional nonlinear flow and transport with buoyancy. *SPE Journal*, **23**, 522–534.

Khait, M. and Voskov, D.V. [2017] Operator-based linearization for general purpose reservoir simulation. *Journal of Petroleum Science and Engineering*, **157**, 990–998.
Khan, M.Y. and Mandal, A. [2020] Analytical model for gravity segregation in WAG displacement recovery of inclined stratified reservoirs. *Journal of Petroleum Science and Engineering*, **186**, 106722.
Lake, L.W., Johns, R., Rossen, W.R. and Pope, G.A. [2014] Fundamentals of enhanced oil recovery.
Leeftink, T., Latooij, C. and Rossen, W. [2015] Injectivity errors in simulation of foam EOR. *Journal of Petroleum Science and Engineering*, **126**, 26–34.
Lyu, X., Voskov, D. and Rossen, W. [2020] Simulation of Foam-Assisted CO2 Storage in Saline Aquifers. In: *ECMOR XVII*, 2020. European Association of Geoscientists & Engineers, 1–16.
Moradi-Araghi, A., Johnston, E., Zornes, D. and Harpole, K. [1997] Laboratory evaluation of surfactants for CO2-foam applications at the South Cowden unit. In: *International Symposium on Oilfield Chemistry*. Society of Petroleum Engineers.
Namani, M., Kleppe, J., Høier, L., Karimaie, H. and Torsæter, O. [2012] Analytical model for zones distributions in non-horizontal miscible WAG injection. *Energy Environ Res*, **2**(2), 159–167.
Redlich, O. and Kwong, J.N. [1949] On the thermodynamics of solutions. V. An equation of state. Fugacities of gaseous solutions. *Chemical reviews*, **44**(1), 233–244.
Rossen, W. [2013] Numerical challenges in foam simulation: a review. In: *SPE annual technical conference and exhibition*. Society of Petroleum Engineers.
Rossen, W. and Stolwijk, G. [2009] Gravity Segregation in Gas IOR in Heterogeneous Reservoirs. In: *IOR 2009-15th European Symposium on Improved Oil Recovery*. European Association of Geoscientists & Engineers, cp–124.
Rossen, W. and Van Duijn, C. [2004] Gravity segregation in steady-state horizontal flow in homogeneous reservoirs. *Journal of Petroleum Science and Engineering*, **43**(1-2), 99–111.
Rossen, W.R. [1996] Foams in enhanced oil recovery. *Foams: Theory, Measurements and Applications*, **57**, 413–464.
Rossen, W.R. and Shen, C. [2007] Gravity segregation in gas-injection IOR. In: *EUROPEC/EAGE conference and exhibition*. Society of Petroleum Engineers.
Rossen, W.R., Van Duijn, C., Nguyen, Q.P., Shen, C. and Vikingstad, A.K. [2010] Injection strategies to overcome gravity segregation in simultaneous gas and water injection into homogeneous reservoirs. *SPE Journal*, **15**(01), 76–90.
Schramm, L.L. [1994] *Foams: fundamentals and applications in the petroleum industry*, 242. American Chemical Society Washington, DC.
Shi, J. and Rossen, W. [1998] Simulation of gravity override in foam processes in porous media. *SPE Reservoir Evaluation & Engineering*, **1**(2), 148–154.
Stone, H.L. [1982] Vertical, conformance in an alternating water-miscible gas flood. In: *SPE annual technical conference and exhibition*. Society of Petroleum Engineers.
Stone, H.L. [2004] A simultaneous water and gas flood design with extraordinary vertical gas sweep. In: *SPE international petroleum conference in Mexico*. Society of Petroleum Engineers.
Talebian, S.H., Masoudi, R., Tan, I.M. and Zitha, P.L. [2013] Foam assisted CO2-EOR; concepts, challenges and applications. In: *SPE Enhanced Oil Recovery Conference*. Society of Petroleum Engineers.
Vitoonkijvanich, S., AlSofi, A.M. and Blunt, M.J. [2015] Design of foam-assisted carbon dioxide storage in a North Sea aquifer using streamline-based simulation. *International Journal of Greenhouse Gas Control*, **33**, 113–121.
Voskov, D.V. [2017] Operator-based linearization approach for modeling of multiphase multi-component flow in porous media. *Journal of Computational Physics*, **337**, 275–288.
Yu, G., Namani, M., Kleppe, J. and Rossen, W. [2017] Gravity Override and Vertical Sweep Efficiency in Dipping Reservoirs. In: *IOR 2017-19th European Symposium on Improved Oil Recovery*, 2017. European Association of Geoscientists & Engineers, 1–10.
Zhou, Z., Rossen, W. et al. [1995] Applying Fractional-Flow Theory to Foam Processes at the" Limiting Capillary Pressure". *SPE Advanced Technology Series*, **3**(01), 154–162.

Appendix: Foam model description

The widely used implicit-texture foam model, named CMG-STARS model (Cheng et al., 2000; CMG-STARS, 2012), is applied to investigate the effects of water saturation (S_w) and surfactant concentration

(W_s) on foam stability. For simplicity, here we list those factors used in these calculations and simulations:

$$k_{rg} = \frac{k^0_{rg}(S_w)}{1 + fmmobF_1F_2} \tag{13}$$

$$F_1 = \begin{cases} \left(\frac{W_s}{fmsurf}\right)^{epsurf} & Ws \leq fmsurf \\ 1 & W_s > fmsurf \end{cases} \tag{14}$$

$$F_2 = 0.5 + \frac{arctan\left[epdry(S_w - fmdry))\right]}{\pi} \tag{15}$$

where $k^0_{rg}(S_w)$ is the gas relative permeability without foam. $fmmob$, $fmdry$, $epdry$, $fmsurf$, and $epsurf$ are foam model parameters. As shown in Eq. (13), gas mobility is reduced in the presence of foam by reducing gas relative permeability in this model. Foam can form whenever water, gas, and surfactant meet in sufficient quantities. We also assume for simplicity that surfactant is already present in the water phase throughout the porous medium.

We use the Corey relative-permeability model in this study. The relative-permeability data of Leeftink et al. (2015) in the absence of foam is used for validating our simulator and investigate the effect of numerical dispersion:

$$k^0_{rg} = 0.8649\left(\frac{1 - S_w - 0.05}{1 - S_{wc} - S_{gr}}\right)^{2.2868} \tag{16}$$

$$k_{rw} = 0.6822\left(\frac{S_w - 0.05}{1 - S_{wc} - S_{gr}}\right)^{2.6844} \tag{17}$$

where the superscript 0 indicates that this is the relative permeability in the absence of foam. In this model, S_{wc}=0.05, and S_{gr}=0.05. With the presence of foam, the foam parameters, $fmmob$, $fmdry$, $epdry$, are 3.14 $\times 10^3$, 0.13, and 1 $\times 10^4$. The data in Table. 2 is used to investigate gravity segregation in heterogeneous reservoirs (from Fig. 10).

The following values are assumed for physical properties in Eq. 1 or Eq. 2: μ_w = 0.001 Pa·s and μ_g = 2.0×10^{-5} Pa·s; ρ_w = 1000 kg/m^3, and ρ_g = 166 kg/m^3 which correspond to the values computed by Redlich-Kwong equation of state (EOS) (Redlich and Kwong, 1949).

To determine the mobility in the mixed zone analytically, it is necessary to calculate S_w from the injected fractional flow f_w:

$$f_w = \frac{1}{1 + \frac{k_{rg}(S_w)}{\mu_g}\frac{\mu_w}{k_{rw}(S_w)}} \tag{18}$$

As shown in Eq. 18 and Fig. 4(a), with a fixed injection water fraction, we can find the corresponding water saturation. This saturation will be used to calculate the mobility in the mixed zone at steady state.